Cancer Cell
Article

Regulation of Tumor Angiogenesis by EZH2

Chunhua Lu,[1,20] Hee Dong Han,[1,20] Lingegowda S. Mangala,[1,20] Rouba Ali-Fehmi,[8] Christopher S. Newton,[9] Laurent Ozbun,[9] Guillermo N. Armaiz-Pena,[1] Wei Hu,[1] Rebecca L. Stone,[1] Adnan Munkarah,[10] Murali K. Ravoori,[2] Mian M.K. Shahzad,[1,11] Jeong-Won Lee,[1,12] Edna Mora,[1,13] Robert R. Langley,[3] Amy R. Carroll,[1] Koji Matsuo,[1] Whitney A. Spannuth,[1] Rosemarie Schmandt,[1] Nicholas B. Jennings,[1] Blake W. Goodman,[1] Robert B. Jaffe,[14] Alpa M. Nick,[1] Hye Sun Kim,[1,15] Eylem Ozturk Guven,[16] Ya-Huey Chen,[17] Long-Yuan Li,[17,18] Ming-Chuan Hsu,[4] Robert L. Coleman,[1,5] George A. Calin,[5,6] Emir B. Denkbas,[16] Jae Yun Lim,[7] Ju-Seog Lee,[7] Vikas Kundra,[2] Michael J. Birrer,[19] Mien-Chie Hung,[4,17] Gabriel Lopez-Berestein,[3,5,6] and Anil K. Sood[1,3,5,*]

[1]Department of Gynecologic Oncology
[2]Department of Experimental Diagnostic Imaging
[3]Department of Cancer Biology
[4]Department of Molecular and Cellular Oncology
[5]Center for RNA and Non-Coding RNA
[6]Department of Experimental Therapeutics
[7]Department of Systems Biology
U.T. M.D. Anderson Cancer Center, 1515 Holcombe Blvd, Unit 950, Houston, TX 77030, USA
[8]Department of Pathology, Wayne State University School of Medicine, Karmanos Cancer Institute, Detroit, MI 48201, USA
[9]Department of Cell and Cancer Biology, National Cancer Institute, Bethesda, MD 20892, USA
[10]Women's Health Services, Henry Ford Health System, Detroit, MI 48202, USA
[11]Baylor College of Medicine, Department of Obstetrics and Gynecology, Houston, TX 77030, USA
[12]Department of Obstetrics and Gynecology, Samsung Medical Center, Sungkyunkwan University School of Medicine, Seoul 135-710, Korea
[13]Department of Surgery, University of Puerto Rico, San Juan, 00935, Puerto Rico
[14]Center for Reproductive Sciences, 505 Parnassus, University of California, San Francisco, CA 94143, USA
[15]Department of Pathology, Cheil General Hospital and Women's Healthcare Center, Kwandong University College of Medicine, Seoul 100-380, Korea
[16]Hacettepe University, Nanotechnology and Nanomedicine Division, Ankara 06532, Turkey
[17]Center for Molecular Medicine and Graduate Institute of Cancer Biology, China Medical University and Hospital, Taichung 40447, Taiwan
[18]Department of Biotechnology, Asia University, Taichung 41354, Taiwan
[19]Department of Medicine, Harvard Medical School, Massachusetts General Hospital Cancer Center, Boston, MA 02114, USA
[20]These authors contributed equally to this work
*Correspondence: asood@mdanderson.org
DOI 10.1016/j.ccr.2010.06.016

SUMMARY

Although VEGF-targeted therapies are showing promise, new angiogenesis targets are needed to make additional gains. Here, we show that increased *Zeste* homolog 2 (EZH2) expression in either tumor cells or in tumor vasculature is predictive of poor clinical outcome. The increase in endothelial EZH2 is a direct result of VEGF stimulation by a paracrine circuit that promotes angiogenesis by methylating and silencing vasohibin1 (*vash1*). *Ezh2* silencing in the tumor-associated endothelial cells inhibited angiogenesis mediated by reactivation of VASH1, and reduced ovarian cancer growth, which is further enhanced in combination with *ezh2* silencing in tumor cells. Collectively, these data support the potential for targeting *ezh2* as an important therapeutic approach.

Significance

In this work, we identify EZH2 as a key regulator of tumor angiogenesis. The increase in endothelial EZH2 is a direct result of VEGF stimulation and indicates the presence of a paracrine circuit that promotes angiogenesis. *Ezh2* silencing in the tumor-associated endothelial cells using siRNA, packaged in the chitosan delivery system, resulted in significant growth inhibition in an orthotopic ovarian cancer model. *Ezh2* silencing in tumor endothelial cells resulted in decreased angiogenesis that was mediated by increased levels of the angiogenesis inhibitor, VASH1. Combined, these data provide a significant conceptual advance in our understanding of the regulation of angiogenesis in ovarian carcinoma and support the potential for targeting *ezh2* as a therapeutic approach.

INTRODUCTION

Targeting the tumor vasculature is a particularly attractive strategy because of the presumed genetic stability of endothelial cells (Folkman, 1990). Anti-angiogenic therapeutic strategies are predicted to be meritorious in ovarian cancer patients based on tumor and endothelial VEGF overexpression, and response characteristics noted in phase II clinical trials (Burger et al., 2007; Jain et al., 2006; Spannuth et al., 2008). As such, seven phase III clinical trials in primary and recurrent disease have completed enrollment or are accruing. However, despite initial responses, most patients eventually experience disease progression. The mechanism for this acquired resistance is not well described, but appears to be due in part to expansion or expression of redundant (Relf et al., 1997) alterations in maturing vasculature (Huang et al., 2004) and epigenetic mechanisms (Kerbel, 2001a; Kerbel et al., 2001b); therefore, new anti-angiogenesis targets are needed.

In search of such targets, we carried out genomic profiling studies of endothelial cells from epithelial ovarian cancer and from their normal counterparts (Lu et al., 2007a). Among the many genes with increased expression in tumor endothelial cells, we focused on the enhancer of Zeste homolog 2 (*ezh2*), a member of the polycomb-group (PcG) proteins. PcG proteins are negative regulators of gene expression and are involved in the stable transmission of the repressive state of their target gene throughout the cell cycle (Cavalli and Paro, 1998; Kingston et al., 1996; Simon, 1995). EZH2, a critical component of the polycomb repressive complex 2 (PRC2), has intrinsic histone methyl transferase (HMTase) activity and has been implicated in the progression and metastasis of several cancers (Cha et al., 2005; Raman et al., 2005). For instance, normalized *ezh2* mRNA transcripts were significantly associated with invasiveness of bladder tumors and were significantly higher in grade 3 versus grades 1 and 2 tumors (Weikert et al., 2005). Similar relationships have been described in breast (Kleer et al., 2003), prostate (Varambally et al., 2002), gastric (Matsukawa et al., 2006), and squamous cell cancers of the oral pharynx (Kidani et al., 2009). The association of EZH2 with the malignant phenotype of many solid tumors and its function as a repressor of gene targets led to the hypothesis that EZH2 could impact specific angiogenic mechanisms of endothelial cell biology. Herein, we focused on EZH2 mediated regulation of vasohibin1 (VASH1), which is an endothelial cell specific and intrinsic negative regulator of angiogenesis (Hosaka et al., 2009; Watanabe et al., 2004).

RESULTS

EZH2 Expression in Human Ovarian Carcinoma

We first examined the clinical significance of EZH2 in 180 epithelial ovarian cancers. Increased tumoral EZH2 (EZH2-T) expression, based on the histochemical score, was noted in 66% of samples and increased expression in the vasculature (EZH2-Endo) was noted in 67% of the samples (Figures 1A and 1C). Increased expression of EZH2-T and EZH2-Endo was significantly associated with high-stage ($p < 0.001$) and high-grade ($p < 0.05$; Table 1) disease. Increased EZH2-T was significantly associated with decreased overall survival (median 2.5 years versus 7.33 years, $p < 0.001$; Figure 1B). Similarly, EZH2-Endo was predictive of poor overall survival (2.33 versus 8.33 years, $p < 0.001$; Figure 1D). On the basis of pathway-analysis predictions from our genomic profiling data comparing endothelial cells from epithelial ovarian cancer with those from normal ovarian tissues (Lu et al., 2007a), we next examined potential associations between EZH2 and VEGF expression and microvessel density (MVD). Tumors with increased VEGF expression had significantly greater prevalence of increased EZH2-Endo expression ($p < 0.001$; Figures 1E and 1F). Moreover, tumors with increased EZH2-Endo expression had significantly greater MVD ($p < 0.001$ by Wilcoxon ranked sums test; Figures 1G and 1H).

VEGF Increases EZH2 Levels in Endothelial Cells

On the basis of our observations from clinical samples, we next asked whether VEGF could directly regulate EZH2 levels in endothelial cells. For these experiments, mouse ovarian endothelial cells (MOEC) were cotransfected with the Renilla luciferase plasmid and firefly luciferase plasmid either with or without the *ezh2* promoter construct. Cells were then treated with VEGF, or conditioned media from SKOV3 ovarian cancer cells (SKOV3-CM). There was a significant increase in *ezh2* promoter activity in endothelial cells in response to VEGF, and conditioned media (Figure 1I). To examine changes in EZH2 message, MOECs were treated as indicated above and *ezh2* mRNA was quantified using real-time reverse transcription-polymerase chain reaction (RT-PCR). *Ezh2* mRNA expression levels were significantly increased in endothelial cells in response to VEGF or SKOV3-CM (Figure 1I). The increases in *ezh2* promoter activity and mRNA levels in response to SKOV3-CM or VEGF were blocked with the VEGFR2 specific antibody DC101. Similarly, increased EZH2 protein levels in response to VEGF were blocked by the anti-VEGFR2 antibody (see Figure S1A available online).

Given that EZH2 levels were noted to be increased in tumor and tumor-associated endothelial cells, we next asked whether there was a correlation between the two compartments in human ovarian carcinoma. Orthogonal regression modeling between these factors described a high coefficient of correlation ($r = 0.83$, $p < 0.001$) (Figure S1B). To address whether tumor derived VEGF affected endothelial EZH2, we utilized an orthotopic model of ovarian cancer metastasis. SKOV3ip1 tumor bearing animals were treated with either control antibody or bevacizumab (selective for human VEGF). After treatment for 2 weeks, the tumors were harvested and tumor and endothelial cells were isolated. Compared to normal endothelial cells, *ezh2* levels were significantly higher in the tumor endothelial cells, and this increase was substantially reduced in the bevacizumab treated samples (Figure S1C). Conversely, bevacizumab had no effect on tumor cell *ezh2* levels (Figure S1D). To examine for direct effects of EZH2 on endothelial cells, we transfected EZH2 into MOEC, and examined for effects on tube formation using in vitro assays. Compared to empty vector controls, EZH2 promoted tube formation ($p < 0.01$), which was only minimally blocked by a VEGFR2 inhibitor (Figure S1E). Similar results were noted with HUVECs (data not shown).

Ezh2 Silencing Increases VASH1 in Endothelial Cells

To determine the mechanism by which EZH2 could promote angiogenesis, we searched a database from a whole genome

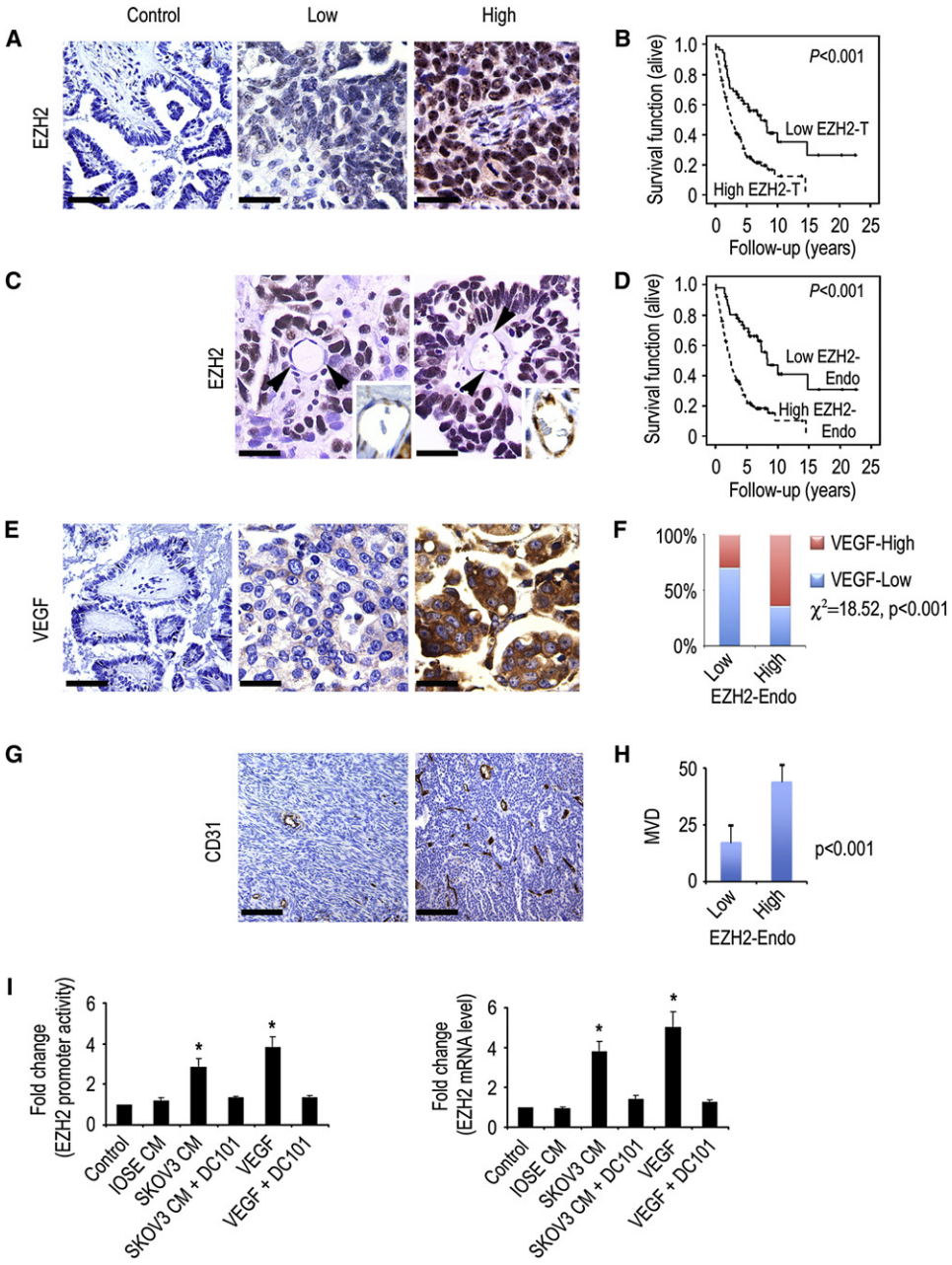

Figure 1. EZH2 Expression in Human Ovarian Carcinoma

(A) Representative images of human tumors with low and high EZH2 expression based on immunohistochemical staining. The scale bar represents 50 μm.

(B) Kaplan-Meier curves of disease-specific mortality for patients whose ovarian tumors expressed high or low levels of EZH2 (EZH2-T). The log-rank test (two-sided) was used to compare differences between the two groups. Increased EZH2-T was significantly associated with decreased overall survival ($p < 0.001$).

(C) Representative images of human ovarian cancer vasculature (arrowheads point to endothelial cells) with low or high immunohistochemical staining for EZH2. The scale bar represents 25 μm. Insets show blood vessels at higher magnification.

(D) Kaplan-Meier curves of disease-specific mortality of patients whose ovarian vasculature expressed low versus high EZH2 (EZH2-Endo). High EZH2-Endo expression was predictive of poor overall survival.

(E) Representative images of human epithelial ovarian cancers with low or high immunohistochemical staining for VEGF. The scale bar represents 50 μm.

(F) VEGF expression was strongly associated with high EZH2-Endo expression levels.

(G) Representative images of human ovarian cancers with low or high immunohistochemical staining for microvessel density (MVD). The scale bar represents 100 μm.

(H) Differences in mean MVD based on EZH2-Endo expression levels in human epithelial ovarian cancers.

(I) VEGF increases *ezh2* in endothelial cells. Results are in response to 6 hr treatment with VEGF (50 ng/mL), or conditioned medium (CM) from the noncancerous ovarian epithelial cell line IOSE120, or the SKOV3 ovarian cancer cells. Fold changes represent the mean of triplicate experiments compared to untreated control cells. *$p < 0.01$. *Ezh2* promoter activity and mRNA levels are increased in mouse ovarian endothelial cells (MOEC) in response to VEGF, or conditioned media from ovarian cancer cells. Error bars indicate SD. See also Figure S1.

Table 1. Association of Clinical and Demographic Features with EZH2 in Epithelial Ovarian Carcinoma

	EZH2-T Overexpression			EZH2-Endo Overexpression		
	No	Yes	p Value	No	Yes	p Value
Mean Age	59.8 years (range 37–89 years)					
Stage						
Low (I/II)	20	9		20	9	
High (III-IV)	41	108	<0.001	37	112	<0.001
Grade						
Low	9	7		10	6	
High	52	112	0.048	47	117	0.005
Histology						
Serous	39	100		35	104	
Other	22	18	0.002	22	18	<0.001

ChIP-on-ChIP analysis that was performed in a separate study. We found that an anti-angiogenic gene, *vash1*, directly binds to *ezh2*. To validate this finding, we performed a ChIP assay of EZH2 for the VASH1 promoter in endothelial cells in the presence or absence of VEGF (Figure 2A), which confirmed direct EZH2 binding to the *vash1* promoter. Quantitative ChIP analysis confirmed the enhanced binding of EZH2 to the *vash1* promoter in response to VEGF (Figure 2B). Next, we silenced the *ezh2* gene in MOECs using two different siRNA sequences (Figure 2C), which resulted in a 3.6- to 3.8-fold increase in *vash1* (Figure 2D). Moreover, there was a significant increase in *vash1* promoter activity after *ezh2* gene silencing (Figure S2).

To determine the mechanism by which EZH2 regulates *vash1*, we performed methylation-specific PCR to detect *vash1* methylation in endothelial cells in the presence of VEGF after silencing *ezh2*. We found that VEGF treatment resulted in a 1.7-fold increase in *vash1* methylation compared to the controls (Figure 2E). However, *ezh2* silencing resulted in a 3.3-fold decrease in VASH1 methylation in the VEGF-treated MOECs. *Ezh2* gene silencing also decreased histone 3 methylation at lysine 27 by 2.5-fold in endothelial cells (Figure 2F).

E2F Mediated Regulation of *Ezh2* in Endothelial Cells

It is known that VEGF can activate E2F transcription factors (Zhu et al., 2003). Due to their suspected role in regulating EZH2 levels, we first tested the effect of VEGF on E2F1-5 in MOECs. There was a significant increase in *e2f1* and *e2f3*,

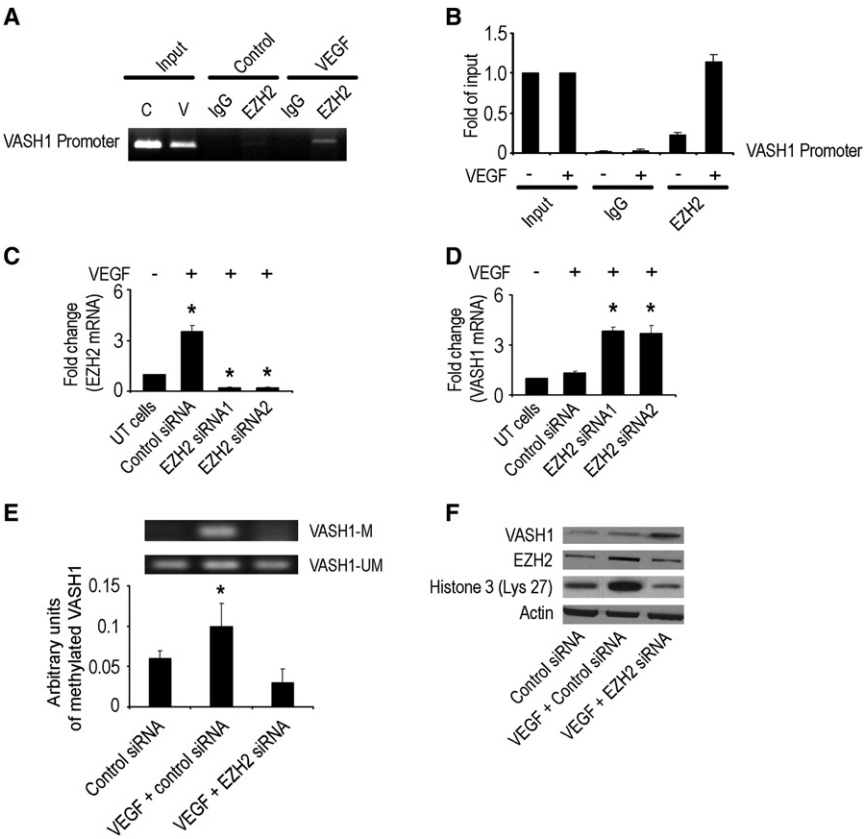

Figure 2. *Ezh2* Gene Silencing Increases *vash1* mRNA Expression in Endothelial Cells

(A) ChIP assay of EZH2 binding to *vash1* promoter in response to VEGF in mouse ovarian endothelial cells (MOEC). Cross-linked chromatin from MOEC was treated with (+) or without (–) VEGF and immunoprecipitated (IP) using EZH2 or mouse IgG antibodies. The input and immunoprecipitated DNA were subjected to PCR using primers corresponding to the 3800–3584 base pairs upstream of *vash1* transcription start site. PCR products were examined on ethidium bromide-stained agarose gel.

(B) Quantitative ChIP assay of EZH2 binding to VASH1 promoter in response to VEGF in endothelial cells. Treatment conditions are similar to those described in (A). PCR products were examined by Roche SYBR Green System for quantitative PCR.

(C) MOECs were transfected with control or mouse *ezh2* siRNA (two different sequences) and harvested after 72 hr. Untransfected (UT) cells were used as controls. RNA was isolated and subjected to real-time quantitative RT-PCR. The fold difference represents the mean of triplicate experiments compared to control siRNA treated cells. *$p < 0.01$.

(D) Fold change in *vash1* mRNA levels in MOEC after transfection with either control or *ezh2* siRNA (two different sequences). *$p < 0.01$.

(E) The effect of *ezh2* gene silencing on *ezh2* methylation in VEGF-treated MOECs was detected by methylation specific PCR. The inhibitory units of methylated *vash1* were normalized by that of the unmethylated *vash1* and represent the mean of triplicate experiments. *$p < 0.05$.

(F) Western blot of lysate collected 48 hr after transfection of MOEC with control, VEGF-treated, and mouse EZH2 siRNA-treated cells. Error bars indicate SEM. See also Figure S2.

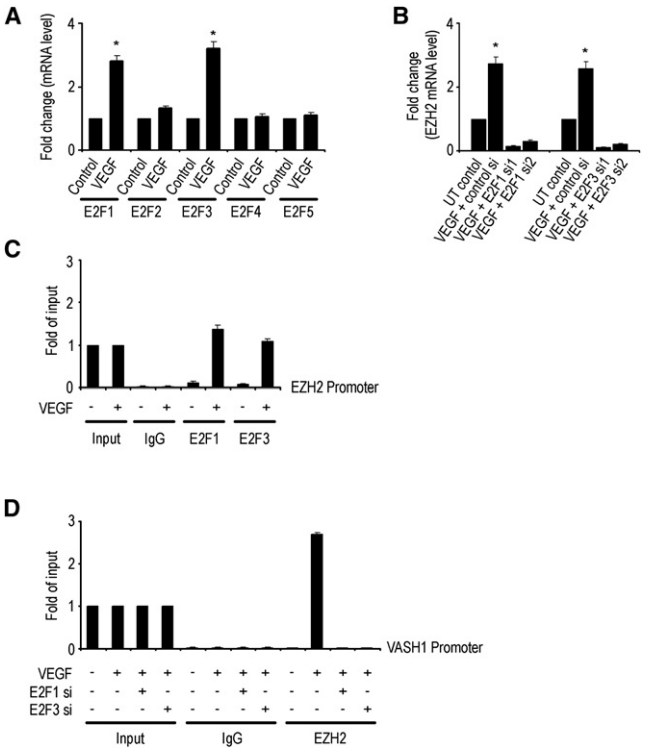

Figure 3. E2F-Mediated Regulation of *ezh2* and *vash1*

(A) Expression levels of *e2f* transcription factors in mouse ovarian endothelial cells (MOEC) after treatment with VEGF. *p < 0.01.

(B) Effect of VEGF and either control, *e2f1*, or *e2f3* siRNA (two different sequences) on *ezh2* mRNA levels. The fold change in levels of mRNA expression represents the mean of triplicate experiments. *p < 0.01.

(C) Quantitative ChIP assay of E2F1 and E2F3 binding to *ezh2* promoter in response to VEGF in MOEC. Crosslinked chromatin from MOECs treated with (+) or without (–) VEGF 50 ng/ml was immunoprecipitated using E2F1, E2F3, or mouse IgG antibodies. The input and immunoprecipitated DNA were subjected to PCR using primers corresponding to the 442–151 base pairs upstream of *ezh2* transcription site. PCR products were examined by Roche SYBR Green System for quantitative PCR.

(D) Crosslinked chromatin from MOECs treated with (+) or without (–) indicated siRNA and with (+) or without (–) VEGF 50 ng/ml was immunoprecipitated using EZH2 or mouse IgG antibodies. The input and immunoprecipitated DNA were subjected to PCR using primers corresponding to the 3800–3584 base pairs upstream of *vash1* transcription site. PCR products were examined by Roche SYBR Green System for quantitative PCR. Error bars indicate SEM. See also Figure S3.

but not others, after treatment with VEGF (Figure 3A). To determine which *e2f* transcription factors might be responsible for increasing *ezh2* levels, we next examined the effects of VEGF after silencing either *e2f1* or *e2f3*. *Ezh2* levels were significantly decreased in *e2f1* and *e2f3* silenced cells (Figure 3B). To validate the binding of *ezh2* promoter to E2F1 and/or E2F3 transcription factors, we performed ChIP assays of *ezh2* to these transcription factors. As shown in Figure 3C, E2F1 and E2F3 bind directly to the *ezh2* promoter, demonstrating that *ezh2* is a direct target of the E2F transcription factors (Wu et al., 2010). Moreover, the VEGF mediated binding of EZH2 to the *vash1* promoter was abrogated with *e2f1* or *e2f3* gene silencing (Figure 3D).

To determine the functional role of VASH1 in angiogenesis, we performed migration and tube formation assays using MOECs after *vash1* gene silencing using two different siRNA sequences. Both cell migration and tube formation were significantly increased after *vash1* gene silencing (Figures S3A and S3B). Similar results were obtained with HUVEC (data not shown).

In Vivo *ezh2* Gene Silencing

On the basis of our in vitro findings, we next asked whether *ezh2* gene silencing in vivo would affect tumor growth and angiogenesis. Before conducting the *ezh2* targeted in vivo experiments, we developed and characterized chitosan (CH) nanoparticles for systemic delivery of siRNA into both tumor cells and tumor-associated vasculature. Several formulations of CH with siRNA (siRNA/CH) were tested (Figure S4A) and optimized (Figures S4B–S4I) and the 3:1 ratio (CH/TPP) nanoparticles showed the greatest (75%) incorporation efficiency (Figure S4D). Therefore, for all subsequent experiments, we used the siRNA/CH3 nanoparticles due to their small size, slight positive charge, and high incorporation efficiency of siRNA.

Prior to performing proof-of-concept in vivo efficacy studies, we tested the efficiency of siRNA delivery into orthotopic ovarian tumors. Nonsilencing siRNA labeled with Alexa-555 was incorporated into CH nanoparticles and injected intravenously (i.v.) into mice bearing HeyA8 orthotopic tumors (17 days after intraperitoneal [i.p.] inoculation of tumor cells). Tumors were harvested at 15 hr and 3, 5, or 7 days (3 mice per time point) after injection and examined for extent of siRNA delivery. At all time points, punctated emissions of the siRNA were noted in the perinuclear regions of individual cells. SiRNA was noted in >80% of fields examined after a single intravenous injection. To confirm delivery of siRNA in the vasculature, we also stained slides for CD31. Indeed, siRNA was delivered into the tumor-associated endothelial cells, suggesting potential applications for targeting the tumor vasculature (Figure 4A). To confirm intracellular delivery of siRNA, we created 3D reconstructions of the tumors using confocal microscopy. Lateral views of the optical sections clearly demonstrated the presence of siRNA within the tumor cells (Figure 4B). However, very little siRNA was taken up by macrophages as determined by labeling tissues with f4/80 (Figure S4J). To examine the biodistribution of siRNA into other organs, we also examined sections of liver, lung, kidney, heart, spleen, and brain, and detected siRNA delivery in most of these organs (Figure S4K). We also utilized optical imaging to assess biodistribution. Fluorescence corresponding to siRNA uptake was seen in tumor and various organs, such as kidney, liver, lung, and spleen (Figure 4C). Semiquantitative assessment of fluorescence confirmed increased uptake of siRNA in HeyA8 tumors and various organs in mice injected i.v. with Cy 5.5 labeled siRNA/CH compared to those injected with unlabeled siRNA/CH (Figure 4D).

To examine the in vivo effects of *ezh2* gene silencing on tumor growth, we used *ezh2* siRNA directed to either the human (tumor cells; *ezh2* Hs siRNA/CH) or mouse (endothelial cells; *ezh2* Mm siRNA/CH) sequence. The expression levels of EZH2 in ovarian cancer cells are shown in Figure S5A; the specificity of siRNA was confirmed by testing each siRNA in both MOEC and human tumor (HeyA8) cells (Figure S5B). After intravenous injection of either control siRNA/CH, *ezh2* Hs siRNA/CH, *ezh2* Mm

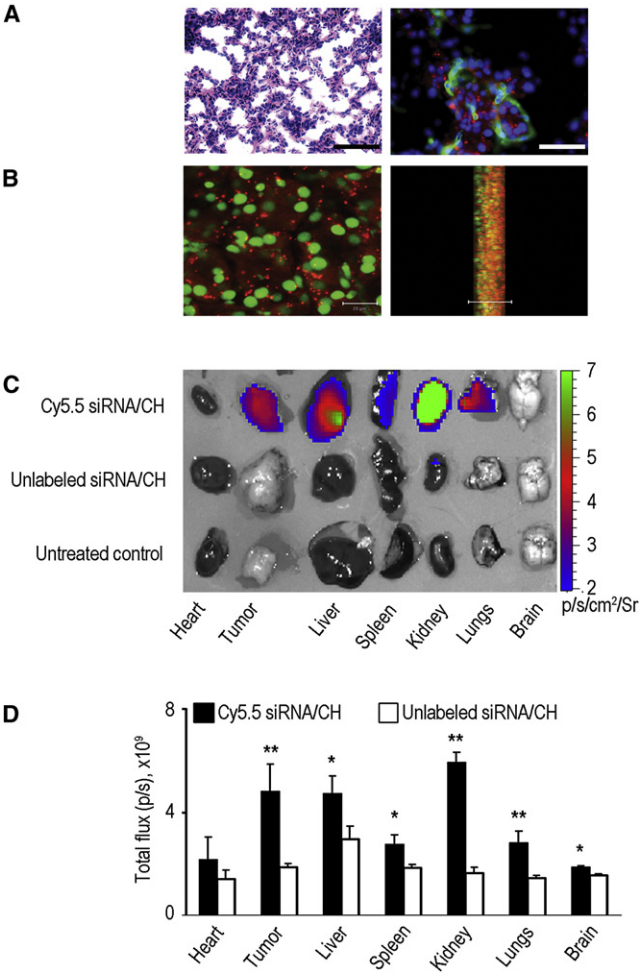

Figure 4. In Vivo siRNA Delivery with Chitosan Nanoparticles

Distribution of siRNA after single intravenous injection of Alexa-555 siRNA/CH nanoparticles in orthotopic HeyA8 tumor bearing nude mice.

(A) Fluorescent siRNA distribution in tumor tissue. Hematoxylin and eosin, original magnification 200× (left); tumor tissues were stained with anti-CD31 (green) antibody to detect endothelial cells (right). The scale bar represents 50 μm.

(B) Fluorescent siRNA distribution in tumor tissue. Sections (8 μm thick) were stained with Sytox green and examined with confocal microscopy (scale bar represents 20 μm) (left); lateral view (right). Photographs taken every 1 μm were stacked and examined from the lateral view. Nuclei were labeled with Sytox green and fluorescent siRNA (red) was seen throughout the section. At all time points, punctated emissions of the siRNA were noted in the perinuclear regions of individual cells, and siRNA was seen in >80% of fields examined.

(C and D) Optical imaging of organs and tumors from HeyA8 tumor-bearing mice treated with either Cy5.5 siRNA/CH or unlabeled siRNA/CH. (C) shows fluorescence intensity overlaid on white light images of different mouse organs and tumor. (D) shows a semiquantitative evaluation of fluorescence intensity in different mouse organs. Error bars indicate SD. *$p < 0.05$;**$p < 0.01$. See also Figure S4.

siRNA/CH, or the combination of *ezh2* targeted siRNAs into HeyA8 tumor-bearing mice (n = 3 mice per group at each time point), tumors were harvested at different time points and examined for EZH2 protein levels. EZH2 levels were decreased by 24 hr after single injection of *ezh2* Hs siRNA/CH with return of expression to baseline expression levels after 96 hr (Figure 5A). *Ezh2* gene silencing was also confirmed with real-time RT-PCR analysis of tumor and endothelial cells (Figures S5D and S5E). To determine the localization of EZH2 silencing after siRNA/CH administration, we performed dual immunofluorescence staining for EZH2 and CD31. This experiment further demonstrated that *ezh2* Hs siRNA/CH resulted in *ezh2* silencing in the tumor cells whereas *ezh2* Mm siRNA/CH silenced *ezh2* only in the tumor endothelial cells (Figure 5B).

To determine the therapeutic efficacy of *ezh2* gene silencing, we used a well-characterized orthotopic model of ovarian carcinoma. Seven days after injection of tumor cells into the peritoneal cavity, mice were randomly allocated to one of the following groups (n = 10 mice per group): (1) control siRNA/CH; (2) *ezh2* Hs siRNA/CH; (3) *ezh2* Mm siRNA/CH; and (4) combination of *ezh2* Hs siRNA/CH plus *ezh2* Mm siRNA/CH. Mice were sacrificed when animals appeared moribund due to significant tumor burden (4–5 weeks after cell injection depending on the cell line). As shown in Figure 5C and Figure S5C, in both models, treatment with *ezh2* Mm siRNA/CH resulted in a significant decrease in tumor burden compared to control siRNA/CH (62% reduction in HeyA8; $p < 0.02$ and 40% reduction in SKOV3ip1, $p < 0.03$). *Ezh2* Hs siRNA/CH as a single-agent had modest effects on tumor growth ($p < 0.04$ for HeyA8; and $p = 0.18$ for SKOV3ip1) compared with control siRNA/CH. However, the greatest reduction was observed with the combination of *ezh2* Hs siRNA/CH plus *ezh2* Mm siRNA/CH (83% reduction in HeyA8, $p < 0.001$ and 65% reduction in SKOV3ip1, $p < 0.001$). To test for potential off-target effects, we tested the efficacy of three additional mouse *ezh2* siRNA sequences with similar effects on tumor growth (data not shown).

To evaluate the effects of EZH2 on other parameters of tumor growth, we examined tumor incidence and number of nodules (Table S1). The combination of *ezh2* Hs siRNA/CH plus *ezh2* Mm siRNA/CH resulted in a significant reduction in tumor nodules in both HeyA8 ($p = 0.002$ versus control siRNA/CH treated group) and SKOV3ip1 tumors ($p = 0.004$ versus control siRNA/CH treated group). The decrease in tumor burden occurred despite having comparable tumor incidence. The mean mouse body weight was similar among the different groups (data not shown), suggesting that feeding and drinking habits were not affected.

Effect of *ezh2* Targeting on Tumor Vasculature and Proliferation

To identify potential mechanisms underlying the efficacy of *ezh2* silencing on ovarian tumors, we examined its effects on several biological end points including MVD, pericyte coverage (DESMIN) and cell proliferation (PCNA). *Ezh2* Mm siRNA/CH and the combination therapy groups had significantly lower microvessel density (Figure 6A) compared to the *ezh2* Hs siRNA/CH and control siRNA/CH treated SKOV3ip1 tumors. Pericyte coverage (assessed with DESMIN and alpha smooth muscle actin [ASMA] staining) was increased in *ezh2* Mm siRNA/CH and the combination groups compared to the other two groups, suggesting greater vascular maturation (Figure 6A and Figure S6B). Combination treatment with *ezh2* Hs siRNA/CH and *ezh2* Mm siRNA/CH also resulted in a significant reduction in cell proliferation (Figure S6C) and increased apoptosis (Figure S6C). Similar

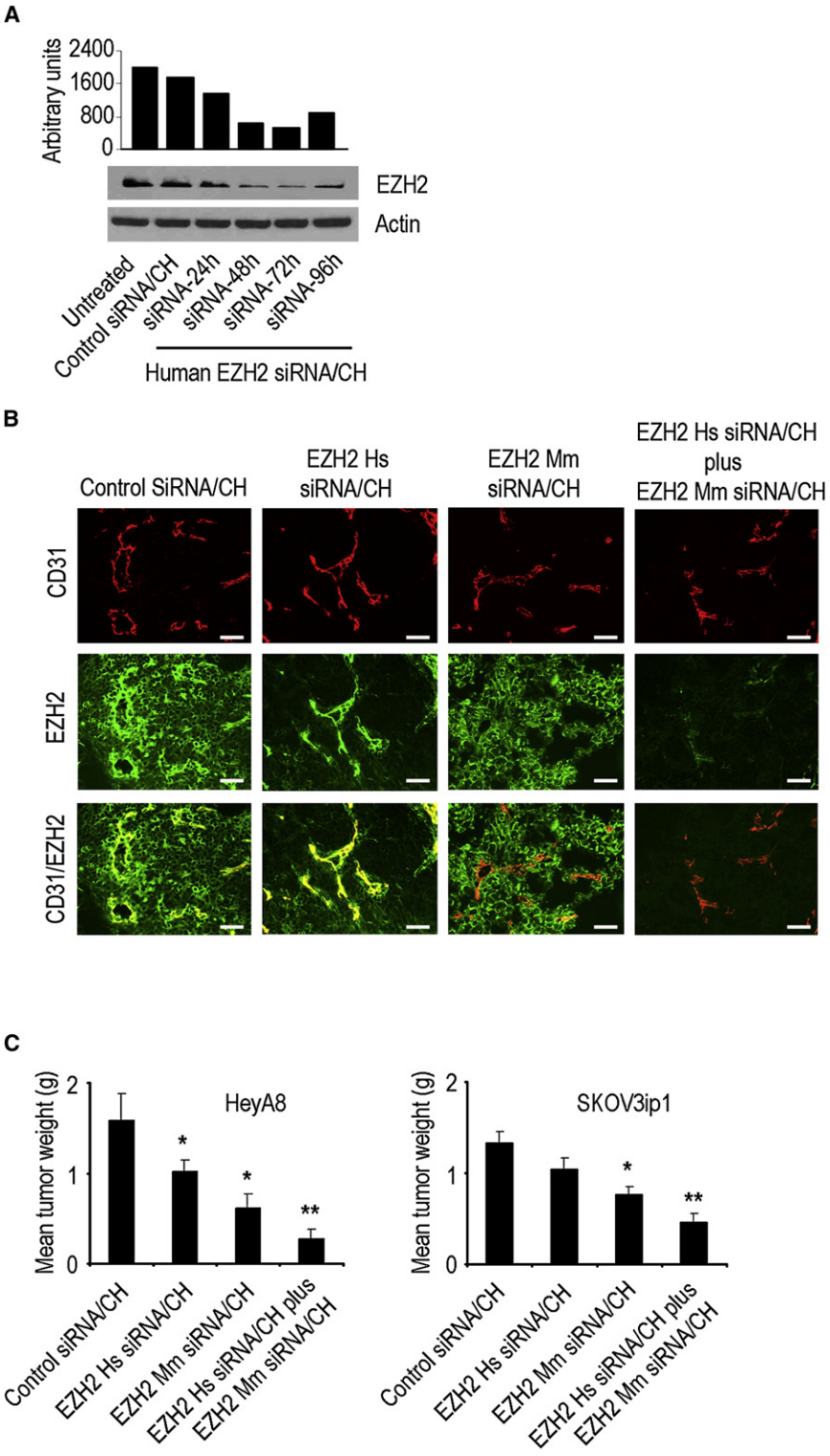

Figure 5. Effects of *ezh2* Gene Silencing on In Vivo Ovarian Cancer Growth

(A) Western blot of lysates from orthotopic tumors collected 24, 48, 72, and 96 hr after a single injection of control siRNA/CH or human (*ezh2* Hs siRNA/CH).

(B) *Ezh2* gene silencing in HeyA8 tumor as well as tumor endothelial cells. Tumors collected after 48 hr of single injection of control siRNA/CH, *ezh2* Hs siRNA/CH, or *ezh2* Mm siRNA/CH and stained for EZH2 (green) and CD31 (red). The scale bar represents 50 μm.

(C) Effects of *ezh2* Hs siRNA/CH or *ezh2* Mm siRNA/CH on tumor weight in orthotopic mouse models of ovarian cancer. Error bars indicate SEM. *$p < 0.05$; **$p < 0.001$. See also Table S1 and Figure S5.

effects of *ezh2* silencing on MVD, pericyte coverage, and proliferation were noted in the HeyA8 model (Figure S6D). To test the effect of *ezh2* gene silencing on intratumor hypoxia, we measured viable hypoxic areas by staining tumor sections with pimonidazole. Compared to control siRNA/CH treated tumors, *ezh2* Mm siRNA/CH treated tumors had modest increase in hypoxia (Figures S6E and S6F), which is consistent with effects of decreased angiogenesis.

Vash1 levels were significantly increased after *ezh2* gene silencing in the tumor endothelial cells (Figure S6A). To determine the requirement for VASH1 in mediating the antitumor effects of *ezh2* silencing, we examined the effects of *vash1* silencing in combination with *ezh2* Mm siRNA/CH. The antitumor effect of *ezh2* silencing in the tumor vasculature was completely reversed by *vash1* silencing (Figure 6B; Table S2), indicating that VASH1 is required for mediating the antitumor effects of *ezh2* silencing.

To determine whether endothelial EZH2 expression is related to VASH1 expression in human epithelial ovarian cancer, we also immunostained 37 samples for VASH1. The best-fit linear regression model demonstrated a significant inverse relationship ($R^2 = -0.59$; $p < 0.001$) between endothelial EZH2 and VASH1 scores (Figure 6C). Specifically, presence of high EZH2 expression was associated with low VASH1 expression, which was otherwise elevated in the absence of or in the presence of low EZH2 expression. We also examined mRNA levels of *ezh2* and *vash1* in endothelial cells isolated from three normal ovarian and ten epithelial ovarian cancer samples using quantitative RT-PCR. Compared to normal ovarian endothelial cells, *vash1* levels were significantly lower in samples with high versus low *ezh2* levels (Figure 6D). To assess vessel maturation (pericyte coverage), the 37 human ovarian cancer samples were immunostained for ASMA. Tumors with low endothelial EZH2

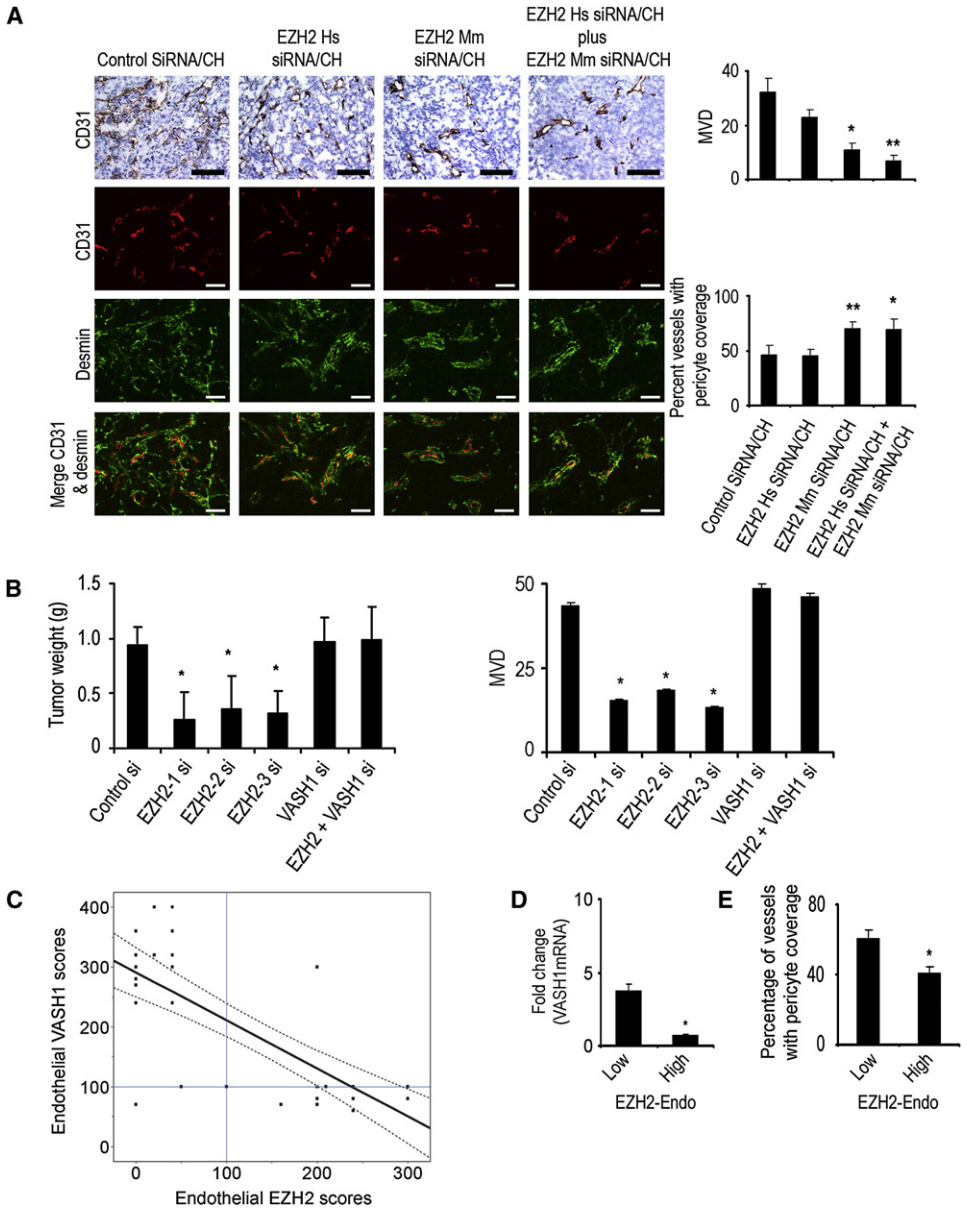

Figure 6. Effect of *ezh2* Targeting on Tumor Vasculature

(A) Effect of tumor (*ezh2* Hs siRNA/CH) or endothelial (*ezh2* Mm siRNA/CH) targeted *ezh2* siRNA on microvessel density (MVD) and pericyte coverage. Tumors harvested after 4–5 weeks of therapy were stained for CD31 (MVD; red) and DESMIN (pericyte coverage; green). The scale bar represents 50 μm. The bars in the graphs correspond sequentially to the labeled columns of images at left. *$p < 0.01$; **$p < 0.001$.

(B) Effects of *vash1* gene silencing on tumor growth in vivo. Nude mice injected with SKOV3ip1 ovarian cancer cells into the peritoneal cavity were randomly divided into six groups (10 mice per group): (1) control siRNA/CH (control si); (2) *ezh2* Mm siRNA1/CH (EZH2-1 si); (3) *ezh2* Mm siRNA2/CH (EZH2-2 si); (4) *ezh2* Mm siRNA3/CH (*ezh2*-3 si); (5) *vash1* Mm siRNA1/CH (*vash1* si); and (6) combination of *ezh2* Mm siRNA1/CH plus *vash1* Mm siRNA/CH. *$p < 0.05$. MVD is shown graphically in the adjacent graph.

(C) Endothelial VASH1 protein expression is plotted against endothelial EZH2 expression in 37 epithelial ovarian cancer specimens. The best-fit linear regression model is depicted with 95% confidence limits ($R^2 = -0.59$, $p < 0.001$). The linear lines intersecting with 100 on each axis represent predetermined cut-off values of "high" versus "low" expression. The presence of EZH2 expression was associated with low expression of VASH1, which was otherwise elevated in the absence of or in the presence of low EZH2 expression.

(D) *Vash1* mRNA levels were measured in endothelial cells isolated from normal ovarian (n = 3), and epithelial ovarian cancer (n = 10) samples using quantitative RT-PCR. The final mRNA levels in the tumor endothelial cells were converted to ratios of decreased (≤1) or increased (>1) relative to levels of mRNA in normal ovarian endothelial cells (*$p < 0.01$).

(E) Vessel maturation was examined by determining the extent of pericyte coverage in human epithelial ovarian cancer samples using an anti-ASMA antibody. *$p < 0.01$. Error bars indicate SEM. See also Table S2 and Figure S6.

had a significantly higher percentage of blood vessels with pericyte coverage ($p < 0.01$; Figure 6E).

To identify potential direct effects of *ezh2* gene silencing on tumor cells, we performed a series of in vitro assays. *Ezh2* siRNA reduced migration by 64% to 71% ($p < 0.01$), and invasion by 63% to 72% ($p < 0.01$) in the SKOV3ip1 cells (Figures S5F and S5G). There were no significant effects on cell viability (Figure S5H). Similar results were noted with the HeyA8 cells (data not shown). To address the potential effects of tumor cell *ezh2* gene silencing on invasion in vivo, we injected SKOV3ip1 tumor cells directly into the ovary and the animals were randomly allocated to the following groups ($n = 10$ mice per group): (1) control siRNA/CH; and (2) *ezh2* Hs siRNA/CH. After 4 weeks of treatment, the mice were dissected and the aggregate tumor weight was 30% lower ($p = 0.03$) in the *ezh2* Hs siRNA/CH treated animals. Although 50% of the mice in the control group developed para-aortic lymph node metastasis, none had nodal metastasis in the *ezh2* Hs siRNA/CH group ($p < 0.001$). Moreover, the ovarian tumors in the control Hs siRNA/CH group had a more infiltrative growth pattern compared to the *ezh2* Hs siRNA/CH group (Figure S5I). To identify genes potentially affected by EZH2 in ovarian cancer cells, we performed genomic analyses of SKOV3ip1 cells after treatment with either control or *ezh2* siRNA. There were 788 genes with significantly increased or decreased expression (Figure S5J). Among these, gene networks of connective tissue growth factor (CTGF) were significantly reduced, which are known to regulate tumor cell migration and invasion (Figure S5K) (Chu et al., 2008; Cicha and Goppelt-Struebe, 2009).

DISCUSSION

Our results describe a mechanism by which VEGF increases EZH2 levels in the tumor vasculature. EZH2, in turn, contributes to tumor angiogenesis by inactivating the antiangiogenic factor, *vash1*, by methylation. These results coupled with pathway-analysis predictions of genomic profiling data of tumor endothelial cells (Lu et al., 2007a) expand our understanding of tumor angiogenesis (Figure 7). Moreover, we have developed and characterized a highly effective method of gene silencing in tumor cells as well as in the blood vessels that support their growth.

PcG proteins play a critical role in determining cell fate during both normal and pathologic processes. Two separate subsets of PcG complexes (PRC1 and PRC2) have been described in humans (Cao and Zhang, 2004). PRC1 is thought to be involved in maintenance of repression, whereas PRC2 plays a role in initiating repression. The PRC2 complex consists of the EZH2, EED, and SUZ proteins (Cao and Zhang, 2004). Altered expression of these proteins has been implicated in cancer pathogenesis (Raman et al., 2005; Cao and Zhang, 2004). However, prior to our work, the role of EZH2 in angiogenesis was not known.

Angiogenesis is regulated by the balance of various proangiogenic stimulators, such as VEGF, and several angiogenesis inhibitors such as angiostatin, and endostatin (Folkman, 1990). On the basis of findings from genomic profiling of endothelial cells from ovarian cancer versus those from normal ovaries, we discovered that EZH2 expression is significantly increased in tumor-associated endothelial cells (Lu et al., 2007a). VEGF is well recognized as a proangiogenic factor in ovarian and other cancers (Spannuth et al., 2008), and its receptors are expressed by endothelial and other cell types including tumor and perivascular cells (Spannuth et al., 2009). In the current study, we showed that VEGF can directly increase EZH2 levels in endothelial cells, which in turn inactivates a potent antiangiogenic factor, VASH1. Silencing *ezh2* gene resulted in demethylation of *vash1* in endothelial cells. This finding is consistent with the role of EZH2 in controlling DNA methylation of EZH2-targeted genes concomitant with reducing H3K27 (McGarvey et al., 2007). VASH1 is known to inhibit endothelial-cell migration, proliferation, and tube formation (Shen et al., 2006). VASH1 expression can be induced by VEGF as part of a negative feedback mechanism in endothelial cells (Hosaka et al., 2009; Tamaki et al., 2009; Watanabe et al., 2004; Yoshinaga et al., 2008). VASH1 limits tumor-associated angiogenesis and increases vessel maturity (Kern et al., 2009). Given that VASH1 levels are low in the setting of high EZH2, *vash1* siRNA alone had no significant effect on tumor growth. However, *vash1* levels in tumor endothelial cells are increased in response to *ezh2* gene silencing, and *vash1* siRNA blocked the inhibitory effects of *ezh2* gene silencing on tumor growth.

A number of therapeutic antiangiogenic targets have recently emerged supporting the clinical rationale of exploiting tumor and endothelial cell interactions. The most mature and promising among ovarian cancer patients involves VEGF and its receptors. For instance, bevacizumab, a chimeric monoclonal antibody targeting VEGF-A has demonstrated impressive single agent activity (objective response and nonprogression at 6 months) in recurrent ovarian cancer patients and more recently, significant efficacy (PFS) in combination with chemotherapy administered in the frontline adjuvant setting (Burger et al., 2007; Burger et al., 2010). However, this compound and others in its class indiscriminately target VEGF, leading to a number of clinically significant and sometimes lethal side effects (Stone et al., 2010). In addition, new strategies targeting angiogenesis are needed as the above therapies are rarely curative and a growing population of patients are demonstrating resistance to anti-VEGF agents. EZH2-targeting represents an innovative strategy, which has activity on both tumor cells and tumor-associated vasculature. The differential expression between normal and tumor vasculature may be hypothesized to have less off-target associated toxicity. Nevertheless, combinatorial approaches with VEGF targeting may augment efficacy and are attractive for further preclinical exploration.

Although a number of important targets in tumor and endothelial cells have been identified, many of these are difficult to target with small molecule inhibitors and monoclonal antibodies. This limitation prompted us to use RNA interference as a means to target *ezh2*. We have recently demonstrated that a neutral nanoliposomal carrier allows efficient systemic delivery of siRNA into orthotopic tumors (Landen et al., 2005; Thaker et al., 2006). However, because of limited delivery of siRNA into the tumor-associated endothelial cells with this approach, we sought to develop additional nanoparticles that would allow siRNA delivery into both tumor and tumor-associated endothelial cells. Chitosan is desirable for biological applications due to properties such as low immunogenicity and low toxicity (Kumar, 2000). These properties make use of chitosan for systemic in vivo siRNA delivery highly attractive (Howard et al., 2006). Indeed,

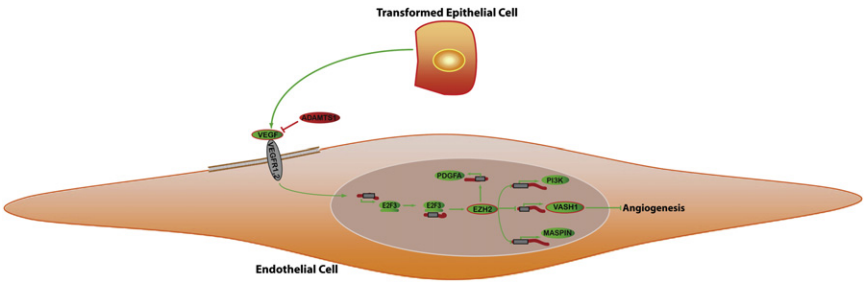

Figure 7. Analysis of Putative *ezh2* Pathways in Cancer-Associated Endothelial Cells

Pathway diagrams were generated with the assistance of Pathway Studio software (Ariadne, Rockville, MD). A model is reported in which VEGF stimulation leads to increased expression of e2f transcription factors, which directly modulates *ezh2* levels. EZH2, a transcriptional repressor, causes *vash1* silencing by promoter methylation and subsequently increases angiogenesis.

our data demonstrate highly effective delivery of siRNA incorporated into chitosan nanoparticles into both tumor and tumor-associated endothelial cells. Such an approach may add a powerful tool to the armamentarium for targeting angiogenesis promoting genes.

In summary, molecular and genetic manipulations have identified EZH2 as a key regulator of tumor angiogenesis here, but these effects do not rule out the possibility that EZH2 has oncogenic functions in tumor cells (Cao and Zhang, 2004; Raman et al., 2005). For example, EZH2 has been implicated in cellular transformation, proliferation, and avoidance of apoptosis (Tonini et al., 2008). However, to the extent that targeting tumor endothelial cells provides therapeutic benefit (Burger et al., 2007; Jain et al., 2006), interfering with EZH2 in the tumor and endothelial cells might represent an important strategy for treatment of ovarian and other cancers.

EXPERIMENTAL PROCEDURES

Cell Lines and Culture

The HeyA8 and SKOV3ip1 human epithelial ovarian cancer cells were maintained as described previously (Kamat et al., 2007; Lu et al., 2007b). The derivation and characterization of the mouse ovarian endothelial cells (MOEC) has been described previously (Langley et al., 2003). HUVECs were purchased from Cambrex (Walkersville, MD) and maintained with heparin and gentamicin/amphotericin-B, as previously described (Ptasinska et al., 2007).

Ezh2 Promoter Construct

The *ezh2* promoter was amplified by PCR from the Roswell Park Cancer Institute human BAC library 11, Clone-ID RP11-992C19 purchased from the Children's Hospital Oakland Research Institute (Oakland, CA), and then cloned into the pGL3-Basic Vector (Promega Corp., Madison, WI). The *ezh2* promoter construct was amplified using primers (see Supplemental Experimental Procedures) with XhoI and HindIII restriction endonuclease sites added to the ends. Purified PCR product was then cloned upstream of the luc+ gene in the pGL3-Basic Vector (Promega Corp.).

Luciferase Reporter Assay

Relative activity of the *ezh2* promoter in MOEC was determined by luciferase reporter assays. Cells were transfected in low-serum medium (0.5% serum) with the firefly luciferase plasmid, either empty vector (pGL3-Basic) or the *ezh2* promoter construct vector (EZH2prom-pGL3-Basic), in 12-well plates using Effectene Transfection Reagent from QIAGEN (Valencia, CA). Cells were then maintained in low-serum medium for 18 hr, washed in PBS, and treated in triplicate at 37°C for 6 hr. Treatments included recombinant human $rhVEGF_{165}$ (VEGF; 50 ng/mL; Peprotech, Rocky Hill, NJ), in fresh medium plus 0.5% serum, and conditioned media from immortalized ovarian surface epithelium (IOSE120) or SKOV3 ovarian cancer cells. After treatment, cells were washed and processed using the Dual-Luciferase Reporter Assay System (Promega).

Chromatin Immunoprecipitation Assay

Cells were cultured in low serum medium (0.5% serum) for 18 hr after being transfected with siRNA for 48 hr and then treated with or without VEGF (50 ng/mL) for 6 hr. After treatment, Chromatin immunoprecipitation (ChIP) assays were performed using EZ ChIP kit (Millipore, Temecula, CA) as described by the manufacturer. In brief, crosslinked cells were collected, lysed, sonicated, and subjected to immunoprecipitation with EZH2 antibody (Cell signaling) or mouse IgG (mIgG) control. Immunocomplexes were collected with protein A/G agarose beads and eluted. Cross-links were reversed by incubating at 65°C. DNA was extracted and purified for PCR using primers (see Supplemental Experimental Procedures) corresponding to the 3800–3697 base pairs upstream of the *vash1* transcription start site.

Real-Time Quantitative PCR

Cells were seeded at 1.0×10^4 cells per well in 96-well plates in complete medium and incubated at 37°C for 24 hr, and then in low-serum medium (0.5% serum) for 18 hr, minus EGF and VEGF supplements where appropriate. Real-time quantitative RT-PCR was performed using 50 ng total RNA isolated from treated cells using the RNeasy Mini Kit (QIAGEN). Relative expression values were obtained using the average of three reference genes and the $2^{-\Delta\Delta CT}$ method as described previously, and normalized to control for percent fold changes (Donninger et al., 2004).

SiRNA Constructs and Delivery

SiRNAs were purchased from QIAGEN, Dharmacon (Chicago, IL), or Sigma-Aldrich (Woodlands, TX). A nonsilencing siRNA that did not share sequence homology with any known human mRNA from a BLAST search was used as control for target siRNA, and the same sequence with Alexa-555 tag was used for determining uptake and distribution in tumor and other organs in vivo. In vitro transient transfection was performed as described previously (Landen et al., 2005).

DNA Extraction and Methylation Analysis

After DNA extraction, methylation analysis was done using a methylation kit (EZ-96 gold; Zymo Research, Orange, CA). MethPrimer software was used for the prediction of CpG island of *vash1* and design of methylation specific primers (methylated *vash1* promoter: 5′-TTAGGGATTTACGTATCGACGT-3′ (forward); 5′-AAACGACAAACTCCAACCG-3′ (reverse); and unmethlyated *vash1* promoter: 5′-TTTTTTTTAGGGATTTATGTATTGATGT-3′ (forward); 5′-CTAAACAACAAACTCCAACCACA-3′ (reverse). PCR conditions were 94°C for 5 min with hot start, then 94°C for 45 s, 56°C for 45 s, and 72°C for 45 s (40 cycles). Image analysis (Scion Image for Windows) was used for semiquantitative measurement of methylated and unmethylated VASH1. Methylated VASH1 was normalized to unmethylated VASH1. The experiments were repeated three times.

Orthotopic In Vivo Model of Ovarian Cancer and Tissue Processing

Female athymic nude mice (NCr-nu) were purchased from the NCI-Frederick Cancer Research and Development Center (Frederick, MD) and maintained as previously described (Landen et al., 2005). All mouse studies were approved by the Institutional Animal Care and Use Committee. Mice were cared for in accordance with guidelines set forth by the American Association for Accreditation of Laboratory Animal Care and the US Public Health Service

Policy on Human Care and Use of Laboratory Animals. For intra-ovarian injection, SKOV3ip1 cells (1×10^6) were injected directly into the left ovarian parenchyma through a left flank incision, as previously described (Lu et al., 2008). For therapy experiments, each siRNA was given twice weekly at a dose of 150 μg/kg body weight. At the time of sacrifice, mouse and tumor weight, number, and distribution of tumors were recorded. Individuals who performed the necropsies were blinded to the treatment group assignments. Tissue specimens were fixed either with formalin, OCT (Miles, Elkhart, IN), or snap frozen in liquid nitrogen.

Immunofluorescence and Confocal Microscopy

Staining for EZH2, CD31, DESMIN, and ASMA was performed using frozen tissue as described previously (Lu et al., 2007b). Pericyte coverage was determined by the percent of vessels with ≥50% coverage of DESMIN- or ASMA-positive cells in five random fields at 200× magnification for each tumor.

Optical Imaging

Nude mice bearing HeyA8 tumors (i.p.) were given Cy 5.5 labeled siRNA/CH (n = 5) or unlabeled siRNA/CH (n = 6) i.v., or nothing (n = 2). Forty-eight hours later, fluorescence imaging of excised tumor and organs was performed using the Xenogen IVIS 200 system. Cy5.5 fluorophore excitation ($\lambda_{excitation}$ = 678 nm) and emission ($\lambda_{emission}$ = 703 nm) filter sets were used. Using Living image 2.5 software, regions of interest (ROI) were drawn for each organ and total flux (photons/second or p/s) was measured as photons/s/cm^2/steradian (p/s/cm^2/Sr).

Western Blot Analysis

Western blot analysis was performed as previously reported (Halder et al., 2006; Landen et al., 2005).

Immunohistochemical Staining

For quantification of MVD in the mouse tumor samples, the number of blood vessels staining positive for CD31 (1:800 dilution, PharMingen, San Diego, CA) was recorded in ten random 0.159 mm^2 fields at 200× magnification (Thaker et al., 2006). All staining was quantified by two investigators in a blinded fashion. For human ovarian cancer samples, immunohistochemistry for EZH2 (1:400 dilution; Zymed, San Francisco, CA), CD34 (1:20 dilution; BioGenex Laboratories, San Ramon, CA (Ali-Fehmi et al., 2005; Des Guetz et al., 2006; Ino et al., 2006), VEGF (1:100 dilution; Santa Cruz Biotechnology, Santa Cruz, CA), DESMIN (1:200 dilution, Dako, Carpinteria, CA), ASMA (1:500 dilution; Abcam, Cambridge, MA), VASH1 (1:200 dilution; Abcam, Cambridge, MA), or NG2 (1:500 dilution, Santa Cruz Biotechnology) was performed, as described previously (Ali-Fehmi et al., 2005). For EZH2 and VEGF, the stained slides were scored by two investigators on the basis of the histochemical score (H-score; >100 defined as high expression and ≤ 100, low expression), according to the method described by McCarty et al. (1985) (Ali-Fehmi et al., 2005; Merritt et al., 2008), which considers both the intensity of staining and the percentage of cells stained. MVD and pericyte coverage in clinical samples was quantified as described above.

Human Ovarian Cancer Specimens

After approval by the Institutional Review Board, 180 paraffin-embedded epithelial ovarian cancer specimens (collected between 1985 and 2004) with available clinical outcome data and confirmed diagnosis by a board-certified gynecologic pathologist were obtained from the Karmanos Cancer Institute tumor bank. The study was exempt from informed consent because it used previously collected residual tissue samples.

Statistical Analysis

Differences in continuous variables were analyzed using the Mann-Whitney rank sum or t test. The relationship between EZH2 expression and MVD was determined using the Wilcoxon ranked sums test. Statistical analyses were performed using SPSS 12.0 for Windows (SPSS, Chicago, IL). A two-tailed $p < 0.05$ was considered statistically significant. Kaplan-Meier survival plots were generated and comparisons made using the log-rank statistic. Bivariate orthogonal regression was used to describe the correlation between tumor and endothelial EZH2 expression (H-score).

ACCESSION NUMBERS

The microarray data have been deposited into NCBI GEO under accession number GSE20381.

SUPPLEMENTAL INFORMATION

Supplemental Information includes Supplemental Experimental Procedures, six figures, and two tables and can be found with this article online at doi:10.1016/j.ccr.2010.06.016.

ACKNOWLEDGMENTS

The authors thank Donna Reynolds, and Fang Wang for their technical expertise and helpful discussion. We also thank Dr. Vickie Williams for reviewing the manuscript. Portions of this work were supported by the NIH (CA 110793, 109298, P50 CA083639, P50 CA098258, CA128797, RC2GM092599), the Ovarian Cancer Research Fund, Inc. (Program Project Development Grant), the DOD (OC073399, W81XWH-10-1-0158, BC085265), NSC-96-3111-B, the Zarrow Foundation, the Marcus Foundation, the Kim Medlin Fund, and the Betty Anne Asche Murray Distinguished Professorship. W.A.S., A.M.N., A.R.C., and R.S. are supported by NCI-DHHS-NIH T32 Training Grant (T32 CA101642). K.M. is supported by the GCF/OCRF Ann Schreiber Ovarian Cancer Research grant and an award from the Meyer and Ida Gordon Foundation 2. M.M.K.S. is supported by the NIH/NICHD WRHR Grant (HD050128) and the GCF-Molly Cade Ovarian Cancer Research Grant. M.C.H. and L.Y.L. are supported by the NSC 97-3111-B-039.

Received: August 10, 2009
Revised: February 15, 2010
Accepted: June 24, 2010
Published: August 16, 2010

REFERENCES

Ali-Fehmi, R., Morris, R.T., Bandyopadhyay, S., Che, M., Schimp, V., Malone, J.M., Jr., and Munkarah, A.R. (2005). Expression of cyclooxygenase-2 in advanced stage ovarian serous carcinoma: correlation with tumor cell proliferation, apoptosis, angiogenesis, and survival. Am. J. Obstet. Gynecol. *192*, 819–825.

Burger, R.A., Sill, M.W., Monk, B.J., Greer, B.E., and Sorosky, J.I. (2007). Phase II trial of bevacizumab in persistent or recurrent epithelial ovarian cancer or primary peritoneal cancer: a Gynecologic Oncology Group Study. J. Clin. Oncol. *25*, 5165–5171.

Burger, R.A., Brady, M.F., Bookman, M.A., Walker, J.L., Homesle, H.D., Fowler, J., Monk, B.J., Greer, B.E., Boente, M., and Liang, S.X. (2010). Phase III trial of bevacizumab (BEV) in the primary treatment of advanced epithelial ovarian cancer (EOC), primary peritoneal cancer (PPC), or fallopian tube cancer (FTC): a Gynecologic Oncology Group Study. J. Clin. Oncol. *28*, 18s.

Cao, R., and Zhang, Y. (2004). The functions of E(Z)/EZH2-mediated methylation of lysine 27 in histone H3. Curr. Opin. Genet. Dev. *14*, 155–164.

Cavalli, G., and Paro, R. (1998). Chromo-domain proteins: linking chromatin structure to epigenetic regulation. Curr. Opin. Cell Biol. *10*, 354–360.

Cha, T.L., Zhou, B.P., Xia, W., Wu, Y., Yang, C.C., Chen, C.T., Ping, B., Otte, A.P., and Hung, M.C. (2005). Akt-mediated phosphorylation of EZH2 suppresses methylation of lysine 27 in histone H3. Science *310*, 306–310.

Chu, C.Y., Chang, C.C., Prakash, E., and Kuo, M.L. (2008). Connective tissue growth factor (CTGF) and cancer progression. J. Biomed. Sci. *15*, 675–685.

Cicha, I., and Goppelt-Struebe, M. (2009). Connective tissue growth factor: context-dependent functions and mechanisms of regulation. Biofactors *35*, 200–208.

Des Guetz, G., Uzzan, B., Nicolas, P., Cucherat, M., Morere, J.F., Benamouzig, R., Breau, J.L., and Perret, G.Y. (2006). Microvessel density and VEGF expression are prognostic factors in colorectal cancer. Meta-analysis of the literature. Br. J. Cancer *94*, 1823–1832.

Donninger, H., Bonome, T., Radonovich, M., Pise-Masison, C.A., Brady, J., Shih, J.H., Barrett, J.C., and Birrer, M.J. (2004). Whole genome expression profiling of advance stage papillary serous ovarian cancer reveals activated pathways. Oncogene *23*, 8065–8077.

Folkman, J. (1990). What is the evidence that tumors are angiogenesis dependent? J. Natl. Cancer Inst. *82*, 4–6.

Halder, J., Kamat, A.A., Landen, C.N., Jr., Han, L.Y., Lutgendorf, S.K., Lin, Y.G., Merritt, W.M., Jennings, N.B., Chavez-Reyes, A., Coleman, R.L., et al. (2006). Focal adhesion kinase targeting using in vivo short interfering RNA delivery in neutral liposomes for ovarian carcinoma therapy. Clin. Cancer Res. *12*, 4916–4924.

Hosaka, T., Kimura, H., Heishi, T., Suzuki, Y., Miyashita, H., Ohta, H., Sonoda, H., Moriya, T., Suzuki, S., Kondo, T., and Sato, Y. (2009). Vasohibin-1 expression in endothelium of tumor blood vessels regulates angiogenesis. Am. J. Pathol. *175*, 430–439.

Howard, K.A., Rahbek, U.L., Liu, X., Damgaard, C.K., Glud, S.Z., Andersen, M.O., Hovgaard, M.B., Schmitz, A., Nyengaard, J.R., Besenbacher, F., and Kjems, J. (2006). RNA interference in vitro and in vivo using a novel chitosan/siRNA nanoparticle system. Mol. Ther. *14*, 476–484.

Huang, J., Soffer, S.Z., Kim, E.S., McCrudden, K.W., New, T., Manley, C.A., Middlesworth, W., O'Toole, K., Yamashiro, D.J., and Kandel, J.J. (2004). Vascular remodeling marks tumors that recur during chronic suppression of angiogenesis. Mol. Cancer Res. *2*, 36–42.

Ino, K., Shibata, K., Kajiyama, H., Yamamoto, E., Nagasaka, T., Nawa, A., Nomura, S., and Kikkawa, F. (2006). Angiotensin II type 1 receptor expression in ovarian cancer and its correlation with tumour angiogenesis and patient survival. Br. J. Cancer *94*, 552–560.

Jain, R.K., Duda, D.G., Clark, J.W., and Loeffler, J.S. (2006). Lessons from phase III clinical trials on anti-VEGF therapy for cancer. Nat. Clin. Pract. Oncol. *3*, 24–40.

Kamat, A.A., Kim, T.J., Landen, C.N., Jr., Lu, C., Han, L.Y., Lin, Y.G., Merritt, W.M., Thaker, P.H., Gershenson, D.M., Bischoff, F.Z., et al. (2007). Metronomic chemotherapy enhances the efficacy of antivascular therapy in ovarian cancer. Cancer Res. *67*, 281–288.

Kerbel, R.S. (2001a). Molecular and physiologic mechanisms of drug resistance in cancer: an overview. Cancer Metastasis Rev. *20*, 1–2.

Kerbel, R.S., Yu, J., Tran, J., Man, S., Viloria-Petit, A., Klement, G., Coomber, B.L., and Rak, J. (2001b). Possible mechanisms of acquired resistance to anti-angiogenic drugs: implications for the use of combination therapy approaches. Cancer Metastasis Rev. *20*, 79–86.

Kern, J., Steurer, M., Gastl, G., Gunsilius, E., and Untergasser, G. (2009). Vasohibin inhibits angiogenic sprouting in vitro and supports vascular maturation processes in vivo. BMC Cancer *9*, 284.

Kidani, K., Osaki, M., Tamura, T., Yamaga, K., Shomori, K., Ryoke, K., and Ito, H. (2009). High expression of EZH2 is associated with tumor proliferation and prognosis in human oral squamous cell carcinomas. Oral Oncol. *45*, 39–46.

Kingston, R.E., Bunker, C.A., and Imbalzano, A.N. (1996). Repression and activation by multiprotein complexes that alter chromatin structure. Genes Dev. *10*, 905–920.

Kleer, C.G., Cao, Q., Varambally, S., Shen, R., Ota, I., Tomlins, S.A., Ghosh, D., Sewalt, R.G., Otte, A.P., Hayes, D.F., et al. (2003). EZH2 is a marker of aggressive breast cancer and promotes neoplastic transformation of breast epithelial cells. Proc. Natl. Acad. Sci. USA *100*, 11606–11611.

Kumar, M.N.V.R. (2000). A review of chitin and chitosan applications. React. Funct. Polym. *46*, 1–27.

Landen, C.N., Jr., Chavez-Reyes, A., Bucana, C., Schmandt, R., Deavers, M.T., Lopez-Berestein, G., and Sood, A.K. (2005). Therapeutic EphA2 gene targeting in vivo using neutral liposomal small interfering RNA delivery. Cancer Res. *65*, 6910–6918.

Langley, R.R., Ramirez, K.M., Tsan, R.Z., Van Arsdall, M., Nilsson, M.B., and Fidler, I.J. (2003). Tissue-specific microvascular endothelial cell lines from H-2K(b)-tsA58 mice for studies of angiogenesis and metastasis. Cancer Res. *63*, 2971–2976.

Lu, C., Bonome, T., Li, Y., Kamat, A.A., Han, L.Y., Schmandt, R., Coleman, R.L., Gershenson, D.M., Jaffe, R.B., Birrer, M.J., and Sood, A.K. (2007a). Gene alterations identified by expression profiling in tumor-associated endothelial cells from invasive ovarian carcinoma. Cancer Res. *67*, 1757–1768.

Lu, C., Kamat, A.A., Lin, Y.G., Merritt, W.M., Landen, C.N., Kim, T.J., Spannuth, W., Arumugam, T., Han, L.Y., Jennings, N.B., et al. (2007b). Dual targeting of endothelial cells and pericytes in antivascular therapy for ovarian carcinoma. Clin. Cancer Res. *13*, 4209–4217.

Lu, C., Thaker, P.H., Lin, Y.G., Spannuth, W., Landen, C.N., Merritt, W.M., Jennings, N.B., Langley, R.R., Gershenson, D.M., Yancopoulos, G.D., et al. (2008). Impact of vessel maturation on antiangiogenic therapy in ovarian cancer. Am. J. Obstet. Gynecol. *198*, 477.

Matsukawa, Y., Semba, S., Kato, H., Ito, A., Yanagihara, K., and Yokozaki, H. (2006). Expression of the enhancer of zeste homolog 2 is correlated with poor prognosis in human gastric cancer. Cancer Sci. *97*, 484–491.

McCarty, K.S., Jr., Miller, L.S., Cox, E.B., Konrath, J., and McCarty, K.S., Sr.. (1985). Estrogen receptor analyses. Correlation of biochemical and immunohistochemical methods using monoclonal antireceptor antibodies. Arch. Pathol. Lab. Med. *109*, 716–721.

McGarvey, K.M., Greene, E., Fahrner, J.A., Jenuwein, T., and Baylin, S.B. (2007). DNA methylation and complete transcriptional silencing of cancer genes persist after depletion of EZH2. Cancer Res. *67*, 5097–5102.

Merritt, W.M., Lin, Y.G., Han, L.Y., Kamat, A.A., Spannuth, W.A., Schmandt, R., Urbauer, D., Pennacchio, L.A., Cheng, J.F., Nick, A.M., et al. (2008). Dicer, Drosha, and outcomes in patients with ovarian cancer. N. Engl. J. Med. *359*, 2641–2650.

Ptasinska, A., Wang, S., Zhang, J., Wesley, R.A., and Danner, R.L. (2007). Nitric oxide activation of peroxisome proliferator-activated receptor gamma through a p38 MAPK signaling pathway. FASEB J. *21*, 950–961.

Raman, J.D., Mongan, N.P., Tickoo, S.K., Boorjian, S.A., Scherr, D.S., and Gudas, L.J. (2005). Increased expression of the polycomb group gene, EZH2, in transitional cell carcinoma of the bladder. Clin. Cancer Res. *11*, 8570–8576.

Relf, M., LeJeune, S., Scott, P.A., Fox, S., Smith, K., Leek, R., Moghaddam, A., Whitehouse, R., Bicknell, R., and Harris, A.L. (1997). Expression of the angiogenic factors vascular endothelial cell growth factor, acidic and basic fibroblast growth factor, tumor growth factor beta-1, platelet-derived endothelial cell growth factor, placenta growth factor, and pleiotrophin in human primary breast cancer and its relation to angiogenesis. Cancer Res. *57*, 963–969.

Shen, J., Yang, X., Xiao, W.H., Hackett, S.F., Sato, Y., and Campochiaro, P.A. (2006). Vasohibin is up-regulated by VEGF in the retina and suppresses VEGF receptor 2 and retinal neovascularization. FASEB J. *20*, 723–725.

Simon, J. (1995). Locking in stable states of gene expression: transcriptional control during Drosophila development. Curr. Opin. Cell Biol. *7*, 376–385.

Spannuth, W.A., Nick, A.M., Jennings, N.B., Armaiz-Pena, G.N., Mangala, L.S., Danes, C.G., Lin, Y.G., Merritt, W.M., Thaker, P.H., Kamat, A.A., et al. (2009). Functional significance of VEGFR-2 on ovarian cancer cells. Int. J. Cancer *124*, 1045–1053.

Spannuth, W.A., Sood, A.K., and Coleman, R.L. (2008). Angiogenesis as a strategic target for ovarian cancer therapy. Nat. Clin. Pract. Oncol. *5*, 194–204.

Stone, R.L., Sood, A.K., and Coleman, R.L. (2010). Collateral damage: toxic effects of targeted antiangiogenic therapies in ovarian cancer. Lancet Oncol. *11*, 465–475.

Tamaki, K., Moriya, T., Sato, Y., Ishida, T., Maruo, Y., Yoshinaga, K., Ohuchi, N., and Sasano, H. (2009). Vasohibin-1 in human breast carcinoma: a potential negative feedback regulator of angiogenesis. Cancer Sci. *100*, 88–94.

Thaker, P.H., Han, L.Y., Kamat, A.A., Arevalo, J.M., Takahashi, R., Lu, C., Jennings, N.B., Armaiz-Pena, G., Bankson, J.A., Ravoori, M., et al. (2006). Chronic stress promotes tumor growth and angiogenesis in a mouse model of ovarian carcinoma. Nat. Med. *12*, 939–944.

Tonini, T., D'Andrilli, G., Fucito, A., Gaspa, L., and Bagella, L. (2008). Importance of Ezh2 polycomb protein in tumorigenesis process interfering with the pathway of growth suppressive key elements. J. Cell. Physiol. *214*, 295–300.

Varambally, S., Dhanasekaran, S.M., Zhou, M., Barrette, T.R., Kumar-Sinha, C., Sanda, M.G., Ghosh, D., Pienta, K.J., Sewalt, R.G., Otte, A.P., et al. (2002). The polycomb group protein EZH2 is involved in progression of prostate cancer. Nature *419*, 624–629.

Watanabe, K., Hasegawa, Y., Yamashita, H., Shimizu, K., Ding, Y., Abe, M., Ohta, H., Imagawa, K., Hojo, K., Maki, H., et al. (2004). Vasohibin as an endothelium-derived negative feedback regulator of angiogenesis. J. Clin. Invest. *114*, 898–907.

Weikert, S., Christoph, F., Kollermann, J., Muller, M., Schrader, M., Miller, K., and Krause, H. (2005). Expression levels of the EZH2 polycomb transcriptional repressor correlate with aggressiveness and invasive potential of bladder carcinomas. Int. J. Mol. Med. *16*, 349–353.

Wu, Z.L., Zheng, S.S., Li, Z.M., Qiao, Y.Y., Aau, M.Y., and Yu, Q. (2010). Polycomb protein EZH2 regulates E2F1-dependent apoptosis through epigenetically modulating Bim expression. Cell Death Differ. *17*, 801–810.

Yoshinaga, K., Ito, K., Moriya, T., Nagase, S., Takano, T., Niikura, H., Yaegashi, N., and Sato, Y. (2008). Expression of vasohibin as a novel endothelium-derived angiogenesis inhibitor in endometrial cancer. Cancer Sci. *99*, 914–919.

Zhu, Y., Jin, K., Mao, X.O., and Greenberg, D.A. (2003). Vascular endothelial growth factor promotes proliferation of cortical neuron precursors by regulating E2F expression. FASEB J. *17*, 186–193.